Variations in Duschinsky rotations in *m*-fluorotoluene and *m*-chlorotoluene during excitation and ionization

Alexander R. Davies, David J. Kemp, Lewis G. Warner, Elizabeth F. Fryer, Alan Rees and Timothy G. Wright[a]

School of Chemistry, University of Nottingham, University Park, Nottingham NG7 2RD, UK

[a] Tim.Wright@nottingham.ac.uk

ABSTRACT

We investigate Duschinsky rotation/mixing between three vibrations for both *m*-fluorotoluene (*m*FT) and *m*-chlorotoluene (*m*ClT), during electronic excitation and ionization. In the case of *m*FT, we investigate both the $S_1 \rightarrow S_0$ electronic transition and the $D_0^+ \leftarrow S_1$ ionization, using two-dimensional laser-induced fluorescence (2D-LIF) and zero-electron-kinetic energy (ZEKE) spectroscopy, respectively; for *m*ClT, only the $D_0^+ \leftarrow S_1$ ionization was investigated, using ZEKE spectroscopy. The Duschinsky mixings are different in the two molecules, owing to shifts in vibrational wavenumber and variations in the form of the fundamental vibrations between the different electronic states. There is a very unusual behaviour for two of the *m*FT vibrations, where apparently different conclusions for the identity of two S_1 vibrations arise from the 2D-LIF and ZEKE spectra. We compare the experimental observations to calculated Duschinsky matrices, finding that these successfully pick up the key geometric changes associated with each electronic transition, and so are successful in qualitatively explaining the vibrational activity in the spectra. Experimental values for a number of vibrations across the S_0, S_1 and D_0^+ states are reported and found to compare well to those calculated. Assignments are made for the observed vibration-torsion ("vibtor") bands, and the effect of ~~the~~ vibrational motion on the torsional potential is briefly discussed.

I. INTRODUCTION

An analysis of the vibrational activity in electronic and photoelectron spectra is often used as a signature of vibrational coupling between fundamentals, overtones, and combination levels. This occurs through anharmonic coupling, which leads to the dispersal, and so delocalization, of internal energy within a molecule – an important aspect to enhancing photostability.[1,2,3,4] Sometimes activity in fundamentals other than that excited can be seen in experimental spectra; however, to first order, vibrational fundamentals do not couple anharmonically. Such activity can be induced by changes in geometry that lead to significant Franck-Condon factors (FCFs), or as a result of a Duschinsky rotation,[5] with cross-activity between vibrations being a signature of the latter. Understanding the intensities of vibrational features in electronic and photoelectron spectra is key to understanding electronic and geometric changes between electronic states. A Duschinsky rotation occurs when the vibrational motions and/or force constants vary significantly between two electronic states; then, each of the affected vibrations in one electronic state has a motion that can be expressed as a linear combination of more than one vibrational motion in the other electronic state. This is sometimes termed the Duschinsky effect, with the resulting vibrations said to have undergone Duschinsky mixing. This would mean, for example, that activity arising when exciting from a particular vibration would be more extensive than expected, owing to the excitation of further vibrations in the final electronic state. Of course, both Franck-Condon (FC) and Duschinsky effects will operate simultaneously, which can complicate the interpretation of the spectra.

Very recently, we published resonance-enhanced multiphoton ionization (REMPI) and zero-electron-kinetic-energy (ZEKE) studies of the low-wavenumber regions of *m*-fluorotoluene (*m*FT)[6] and *m*-chlorotoluene (*m*ClT),[7] which mainly focused on torsions and vibration-torsion (vibtor) levels. The *m*FT study complemented the two-dimensional laser-induced fluorescence (2D-LIF) study of Stewart et al., who examined the first 350 cm^{-1} of the $S_1 \leftarrow S_0$ transition.[8] The spectra of both molecules were assigned in terms of torsion and vibtor levels in the S_0 and S_1 states. Earlier, Ito and coworkers[9,10,11,12] reported laser-induced fluorescence (LIF), dispersed fluorescence (DF), REMPI, and ZEKE spectra of the low-wavenumber region of *m*FT. In addition, Ichimura et al.[13] have published LIF and DF spectra of *m*ClT, while Feldgus et al.[14] only reported REMPI and ZEKE spectra of *m*ClT, restricted to the torsional region.

In the present work, we focus on a set of three vibrations that are active in the $S_1 \leftarrow S_0$ transition, and are found to have a high degree of cross-activity, as ascertained using 2D-LIF and ZEKE spectroscopy.

These three vibrations are designated D_{18}, D_{19} and D_{20}, as described in Ref. 15, and whose explicit motions will be discussed later.

II. EXPERIMENTAL

The ZEKE[16] and 2D-LIF[17] apparatuses are the same as those employed recently. In both experiments for *m*FT, a free-jet expansion of *m*FT (Sigma-Aldrich, 98% purity) in 1.5 bar Ar was employed. For the ZEKE experiments on *m*ClT, a free jet expansion was also used, consisting of *m*ClT (Alfa Aesar, 98% purity) in 2 bar Ar, where the *m*ClT sample was heated to ~50°C in order to introduce sufficient vapour to the expansion.

For the 2D-LIF spectra, the free-jet expansion was intersected at X/D ~20 by the frequency-doubled output of a single dye laser (Sirah CobraStretch), operating with Coumarin 503 and pumped with the third harmonic of a Surelite III Nd:YAG laser. The fluorescence was collected, collimated, and focused onto the entrance slits of a 1.5 m Czerny-Turner spectrometer (Sciencetech 9150) operating in single-pass mode, dispersed by a 3600 groove/mm grating, and ~300 cm^{-1} windows of the dispersed fluorescence collected by a CCD camera (Andor iStar DH334T). At a fixed grating angle of the spectrometer, the excitation laser was scanned, and at each excitation wavenumber the camera image was accumulated for 2000 laser shots. This allowed a plot to be produced of fluorescence intensity versus both the excitation laser wavenumber and the wavenumber of the emitted and dispersed fluorescence, termed a 2D-LIF spectrum. [18,19]

For the ZEKE spectra, the focused, frequency-doubled outputs of two dye lasers (Sirah CobraStretch) were overlapped spatially and temporally, and passed through a vacuum chamber coaxially and counterpropagating, where they intersected the free jet expansion. The excitation laser operated with Coumarin 503 and was pumped with the third harmonic (355 nm) of a Surelite III Nd:YAG laser, while the ionization laser operated with Pyrromethene 597, pumped with the second harmonic (532 nm) of a Surelite I Nd:YAG laser. The jet expansion passed between two biased electrical grids located in the extraction region of a time-of-flight mass spectrometer, which was employed in the REMPI experiments. These grids were also used in the ZEKE experiments by application of pulsed voltages, giving typical fields of ~10 V cm^{-1}, after a delay of up to 2 μs; this delay was minimized while avoiding the introduction of excess noise from the prompt electron signal. The resulting ZEKE bands had widths of ~5-7 cm^{-1}. Electron and ion signals were recorded on separate sets of microchannel plates.

III. RESULTS AND ASSIGNMENTS

A. Nomenclature and labelling

1. Vibrational and Torsional Labelling

We shall employ the D_i labels[15] for the vibrations, as used in Refs. 6, 7 and 8, since neither Wilson[20]/Varsányi[21] nor Mulliken[22]/Herzberg[23] notations are appropriate for the vibrations of *m*FT or *m*ClT. The C_s point group labelling scheme[15] is based on the vibrations of the *meta*-difluorobenzene (*m*DFB) molecule.

We shall also refer to the methyl torsional motion for *m*FT and *m*ClT, for which the G_6 molecular symmetry group (MSG) is appropriate, and we shall use those symmetry labels throughout. The torsional levels will be labelled via their *m* quantum number,[6,8] and the correspondence between the C_s point group labels and the G_6 MSG ones is given in Table I. To calculate the overall symmetry of a vibtor level, it is necessary to use the corresponding G_6 label for the vibration, and then find the direct product with the symmetry of the torsion (Table I), noting that a C_{3v} point group direct product table can be used, since the G_6 MSG and the C_{3v} point group are isomorphic.

Under the free-jet expansion conditions employed here, almost all of the molecules are expected to be cooled to their zero-point vibrational level, and thus essentially all $S_1 \leftarrow S_0$ pure vibrational excitations are expected to originate from this level. In contrast, owing to nuclear-spin and rotational symmetry, the molecules can be in one of the $m = 0$ or $m = 1$ torsional levels,[24] with residual population in the $m = 2$ levels also seen.[6,7,8]

2. Transitions

When designating excitations, we shall generally omit the lower level, since it will be obvious from either the jet-cooled conditions or the specified intermediate level. In the usual way, vibrational transitions will be indicated by the cardinal number, *i*, of the D_i vibration, followed by a super-/subscript specifying the number of quanta in the upper/lower states, respectively; torsional transitions will be indicated by *m* followed by its value. Finally, vibtor transitions will be indicated by a combination of the vibrational and torsional transition labels.

As has become common usage, we will generally refer to a level using the notation of a transition, with the level indicated by the specified quantum numbers, with superscripts indicating levels in the S_1 state and, when required, subscripts indicating levels in the S_0 state. Since we will also be referring to transitions and levels involving the ground state cation, D_0^+, we shall indicate those as superscripts, but with a single, additional, preceding superscripted "+" sign. Relative wavenumbers of the levels will be given with respect to the relevant zero-point vibrational level with $m = 0$ in each electronic state.

For cases where the geometry and the torsional potential are both similar in the S_1 and D_0^+ states, the most intense transition is usually expected to be that for which no changes in the torsional and/or vibrational quantum numbers occur: designated as $\Delta m = 0$, $\Delta v = 0$ or $\Delta(v, m) = 0$ transitions, as appropriate. However, as will be seen (and as reported in Refs. 6, 7, 12 and 14), the $\Delta m = 0$ and $\Delta(v, m) = 0$ transitions are almost always not the most intense bands in the ZEKE spectra for *m*FT and *m*ClT, indicative of a significant change in the torsional potential upon ionization.

B. Overview of REMPI spectra

In Figure 1 we show the REMPI spectra of the first 500 cm^{-1} above the origin of the $S_1 \leftarrow S_0$ transition in *m*FT and *m*ClT. The 0–350 cm^{-1} region of the *m*FT spectrum has been discussed in detail previously, in terms of 2D-LIF and ZEKE spectroscopy,[6,8] while the corresponding region of the *m*ClT spectrum has also been discussed relating to ZEKE spectroscopy.[7] Because of the consistent vibrational labelling used for both molecules,[15] it can be seen that the activity in both spectra is similar. In the present work, we shall concentrate on the two expanded regions of Figure 1, between 400–480 cm^{-1} for *m*FT and 350–470 cm^{-1} for *m*ClT. In the case of *m*ClT, the spectrum was recorded in two mass channels, corresponding to the ^{35}Cl and ^{37}Cl isotopologues, where some bands around 370 cm^{-1} can be seen to undergo isotopic shifts (compare the red and black traces in the expanded region in the lower portion of Figure 1), but there are essentially no shifts for the lower-wavenumber bands.[7] For both *m*FT and *m*ClT, these regions are dominated by activity involving three vibrations, D_{18}, D_{19} and D_{20}. As we shall see below, these vibrations are significantly Duschinsky mixed in the S_1 state.

We shall firstly concentrate on the assignment of the 2D-LIF and ZEKE spectra of *m*FT, before moving on to the ZEKE spectrum of *m*ClT (no 2D-LIF spectra were recorded for this molecule). We shall then discuss the observations for both molecules.

C. 2D-LIF and ZEKE spectra of *m*FT

In Figure 2, the 2D-LIF spectrum of *m*FT in the range 412–464 cm^{-1} is presented, while ZEKE spectra recorded at various excitation positions across the same region are shown in Figure 3. Calculated wavenumbers for a selection of pertinent vibrations for both molecules, and for the three different electronic states considered, are presented in Table II – the level of theory utilized has generally been shown to be sufficient for these molecules in our previous work.

It will be seen in the discussion below that the D_{19} and D_{20} vibrations become very mixed in the S_1 state. For this reason, we have designated the S_1 mixed vibrations, D_X and D_Y in the following. The strongest features in the 2D-LIF spectrum (Figure 2) are seen when exciting via 18^1, X^1 and Y^1, each comprising m = 0 and m= 1 components, as indicated; significant cross-activity is evident. The strong emission bands seen when exciting via 18^1 are partially overlapped with those seen when exciting via Y^1. Associated with each of the strong emission bands is a series of vibtor transitions, which have distinctive structure, as seen in the low wavenumber region.[8] These consist of strong $m_{3(+)}$ and weaker $m_{3(-)}$ bands when exciting via the m = 0 components, as well as a strong m_2 band, with weaker m_4 and m_5 bands, when exciting via the m = 1 components – some of these are overlapped by other features in the 2D-LIF spectrum.

In Figure 3, we present the ZEKE spectra recorded via the m = 0 and m = 1 components of the 18^1, X^1 and Y^1 vibrations of *m*FT. It can be seen from Figure 1 that the X^1m^0 and 18^1m^1 transitions overlap, and so the ZEKE spectrum recorded for these overlapped features is included in both the upper and lower portions of Figure 3, but located on the correct scale in each case. Again, significant cross activity is seen when exciting via 18^1, X^1 and Y^1, for both m levels.

To aid in the understanding of the activity of the spectra, Duschinsky matrices were calculated (using the FC-LAB II program)[25] for a selection of the vibrations. This was done for the three pairings of the S_0, S_1, and D_0^+ electronic states for *m*FT, and these are shown in Figure 4. Additionally, we show the calculated motions of the three Duschinsky-mixed vibrations of interest, in each of the three electronic states. First, we point out that the D_i labels are defined with respect to the S_0 motion. (The motions of *meta*-disubstituted benzenes in the S_0 state, on which the D_i labelling is based, were discussed in detail in Ref. 15.) Secondly, the S_0/D_0^+ matrix indicates that the vibrational motions in the ground state cation are very similar to those in the ground state neutral molecule, so that the S_0 vibrational labels, D_i, can also be used for the cationic vibrations to a very good approximation. (It is highlighted that the

wavenumber ordering of the D_{19} and D_{20} vibrations have switched in the cation relative to the S_0 state – see Table II.)

We now turn to the S_0/S_1 matrix for *m*FT in Figure 4. This indicates that the motions of the S_1 vibrations corresponding to the D_{18}, D_{19}, and D_{20} S_0 vibrations are significantly altered, and each of these S_1 vibrations can be thought of as being significant admixtures of the corresponding S_0 ones, i.e. they are Duschinsky mixed; a similar picture holds when these S_1 vibrations are expressed in terms of the D_0^+ vibrations. In contrast, the D_{17} and D_{21} vibrations exhibit extremely similar motions in the three electronic states, and so are not considered to be Duschinsky mixed. We now point out that the S_1 D_{18} vibration is dominated by the same motion as in the S_0 state (and D_0^+ state) and so these are recognizably the same vibration, even though the S_0 and S_1 motions are not precisely the same, with a noteworthy contribution in S_1 from D_{19}. Hence, we retain the D_{18} label for this vibration across the three electronic states. This is not true for the D_{19} and D_{20} vibrations, where the two S_1 vibrations have motions that can be expressed as significant admixtures of the corresponding S_0 (or D_0^+) vibrations; as such, the D_{19} and D_{20} labels cannot be used for these two S_1 vibrations, which is why we have designated them D_X and D_Y, in increasing wavenumber order.

We now look at the activity in the 2D-LIF and ZEKE spectra in more detail. In Figure 2, we can see that there is significant cross activity in the 2D-LIF spectrum involving the D_{18}, D_{19} and D_{20} vibrations, as indicated by the (X^1, 18_1), (X^1, 19_1) and (X^1, 20_1) bands, together with (Y^1, 18_1), (Y^1, 19_1) and (Y^1, 20_1), which appear for each of the two *m* levels. A definite (18^1m^0, 19_1m_0) band can be seen, as well as (18^1m^0, 18_1m_0), but there is only the faintest activity for (18^1m^0, 20_1m_0); there do, however, appear to be ($Y^1m^{0,1}$, $18_1m_{0,1}$) bands, albeit overlapped by (Y^1m^1, 20_1m_4); indicating a lesser contribution of D_{18} to the S_1 state Y^1 vibration, compared to the X^1 vibration – see further discussion below.

With regard to the *m*FT ZEKE spectra in Figure 3, clear $^+19^1$ and $^+20^1$ activity can be seen when exciting via each of X^1 and Y^1, for both $m = 0$ and $m = 1$ levels, with the $^+19^1$ wavenumber being *lower* than that of $^+20^1$, i.e. the opposite order to the S_0 and S_1 states – see Table II. (There is also $^+18^1$ activity, but this is less prominent.) The $^+19^1m^x$ vibtor activity is greatest when exciting via Y^1 and that of $^+20^1m^x$ when exciting via X^1, with this being most clear from the $^+19^1m^{3(+)}$ and $^+20^1m^{3(+)}$ bands. The dual activity of both vibrations is consistent with the vibrational character of the D_X and D_Y vibrations in the S_1 state being highly mixed versions of the corresponding D_0^+ vibrations. The assignment of the various vibtor transitions is relatively straightforward, with the $^+20^1m^x$ transitions being very close to the expected positions; however, the $^+19^1m^x$ bands are somewhat shifted from the expected positions, but can be

identified by their relative intensities and by comparison to the $^{+}20^{1}m^{x}$ bands. Further discussion on the shifted $^{+}19^{1}m^{x}$ band spacings for *m*FT is given in Section IV.B.

At this point, we note that for a symmetric, disubstituted benzene, such as *m*DFB, the point group is C_{2v}, where the D_{19} and D_{20} vibrations are both of b_2 symmetry, while D_{18} is of a_1 symmetry; thus, D_{19} and D_{20} can be thought of as mixing with one another during their evolution as the mass of the substituents changes,[15] while D_{18} cannot. In the asymmetric *m*FT, we note that the masses of CH_3 and a fluorine atom are very similar, and this may be an explanation of why there is strong Duschinsky mixing between D_{19} and D_{20}. Also, as the mass difference between the two substituents increases for an asymmetric disubstitution, D_{18} and D_{19}, evolve into localized motions containing symmetric and asymmetric stretches, respectively, each involving the substituents, both being of a' symmetry (in the C_s point group).[15] In the present case, this is exhibited as the mixing between the D_{18} and D_{19} modes, for which the localization of the motion is not complete, and the extent of this varies between the electronic states (see Figure 4). We now compare and contrast the activity in the 2D-LIF and ZEKE spectra seen when exciting via the 18^1, X^1 and Y^1 levels.

The initial interpretation of the 2D-LIF spectrum (Figure 2) is that D_Y in the S_1 state is dominated by S_0 D_{20} character, with a sizeable contribution from D_{19} and a smaller one from D_{18}; furthermore, D_X has the largest contribution from D_{19} but with large contributions from D_{18} and (to a lesser extent) D_{20}. We can also see that D_{18} in the S_1 state has a significant contribution from S_0 D_{19}. These conclusions are largely in line with the calculated S_0/S_1 Duschinsky matrix (Figure 4).

If we now look at the ZEKE spectra in Figure 3, then we would reach a different conclusion, in that exciting via Y^1 gives the largest contribution from $^{+}D_{19}$ (i.e. the D_{19} vibration in the cation) with a significant contribution from $^{+}D_{20}$, while exciting via X^1 gives the largest contribution from $^{+}D_{20}$, with a significant contribution from $^{+}D_{19}$. Again, these conclusions are in line with the calculated S_1/D_0^{+} Duschinsky matrix – see Figure 4. As a consequence, at first sight it seems that the conclusions from the 2D-LIF and ZEKE spectra are contradictory with regards to the make-up of the D_X and D_Y S_1 vibrations. This must arise from the small, but notable, differences in the motions of the D_{18}, D_{19} and D_{20} vibrations in the S_0 and D_0^{+} electronic states, which cause the expression of the S_1 motions as admixtures of these vibrations in the different electronic states to differ. In addition, the Franck-Condon factors between the vibrations and associated vibtor levels will differ for the $S_1 \rightarrow S_0$ and $D_0^{+} \leftarrow S_1$ transitions, depending on the main geometry changes between the respective pair of electronic states. These have been discussed previously[6,7] for *m*FT and *m*ClT, where the changes are very similar.

Notably, for *m*FT, the C-CH_3 and C-F bond lengths both increase significantly during the $S_1 \rightarrow S_0$ transition; however, the C-CH_3 bond length is almost unchanged during the $D_0^+ \leftarrow S_1$ ionization, while the C-F bond shortens. Also, a shortening of all ring C-C bond lengths occurs during the $S_1 \rightarrow S_0$ transition, while there is an asymmetric change in those bond lengths during the $D_0^+ \leftarrow S_1$ ionization. These are consistent with the 18^1, X^1 and Y^1 activity seen during the $S_1 \leftarrow S_0$ and $S_1 \rightarrow S_0$ transitions (Figure 1 and Figure 2, respectively) and the activity of $^+18^1$ in the ZEKE spectra via the vibrationless m^0 and m^1 levels (see Ref. 6).

We now consider the calculated motions of these three vibrations. Looking first at D_{18} and D_{19} (Figure 4), we see motions in the S_0 and D_0^+ states that have significant in-phase C-CH_3 and C-F stretches for D_{18}, but these are out-of-phase for D_{19}; moreover, the motions of the other atoms are very similar for these states. For D_{18} in the S_1 state, although the motion of the methyl group, and that of some of the ring carbon atoms, is different than those of the other two electronic states, it is dominated by the in-phase C-CH_3 and C-F stretches: this is our justification for employing the same vibrational label. Similarly, for D_{20} in the S_0 and D_0^+ states, the motion can be identified by the in-phase, in-plane bending of the C-CH_3 and C-F bonds. However, in the S_1 state, the motions of two of the vibrations, the ones labelled X and Y, can be seen to be significant mixtures of the motions of the D_{19} and D_{20} vibrations. In particular, the motions of the C-CH_3 and C-F bonds for D_X and D_Y are similar to those of D_{19} and D_{20}, respectively, while the motions of the carbon atoms in the aromatic rings for D_X and D_Y largely resemble D_{20} and D_{19}, respectively. Thus, different aspects of the D_X and D_Y motions resemble different parts of the D_{19} and D_{20} vibrations. This shows that the D_{19} and D_{20} motions have indeed become mixed in S_1, in line with the Duschinsky matrices (Figure 4) and this is reflected in the activity in the 2D-LIF and ZEKE spectra (Figure 2 and Figure 3). Of course, each entry in the Duschinsky matrix is a distillation of the comparisons of all angular and radial displacements between two vibrations; nonetheless, even though the subtleties of the different changes are not necessarily evident, the entry is expected to reflect the most important geometry changes for a particular electronic transition. This case shows that in fact the Duschinsky matrix does give a good qualitative picture of the observed spectral activity, although, for very mixed vibrations, caution is merited in the interpretation of the matrix in establishing how vibrations of one electronic state map onto another. Clearly, for the $S_1 \rightarrow S_0$ emission, it is the motions of the C-CH_3 and C-F bonds that dominate the overlap of the S_1 D_X and D_Y vibrations with the S_0 D_{19} and D_{20} ones; while for the $D_0^+ \leftarrow S_1$ ionization, the relative motions of the carbon atoms in the aromatic ring are the more important in determining the activity.

Summarizing, we conclude that the D_{18}, D_X and D_Y vibrations are heavily mixed in the S_1 state, with the D_{19} and D_{20} contributions to X^1 and Y^1 each being particularly significant; however, when distilled into Duschinsky matrix entries, these are different when expressed in terms of the S_1 or D_0^+ vibrations, but in agreement with the observed vibrational activity.

D. ZEKE spectra of *m*ClT

ZEKE spectra of *m*ClT were recorded when exciting at various positions in the region indicated in the expanded view in the bottom half of Figure 1. These spectra are shown in Figure 5, for the $m = 0$ and $m = 1$ components, respectively; note that the 19^1m^1 and 20^1m^0 transitions overlap, and so the spectrum recorded for these overlapped features is included in both the upper and lower portions of the figure, each shifted to be on the correct relative wavenumber scale. The S_0/D_0^+ Duschinsky matrix shown in Figure 6 indicates that although the D_{18}, D_{19}, and D_{20} vibrations of the D_0^+ state are mixed versions of the corresponding S_0 ones, there is sufficient dominant character to employ the same labels for both states, notably with respect to the motions of the C-CH_3 and C-Cl bonds. With regard to the aromatic ring carbon atoms, although the motions are not the same in the S_1 state as the other two states, they are largely correspondent with that expected for the D_{19} or D_{20} vibrations and this gives a more diagonal Duschinsky matrix, allowing the same vibrational labels to be used in the three states. Although the 2D-LIF spectrum was not recorded, the S_0/S_1 Duschinsky matrix indicates that there would likely be significant cross activity between the 19_1 and 20_1 emissions, but with 18_1 being largely pure.

For *m*ClT, the ZEKE spectra recorded via 19^1m^0 and 19^1m^1 are relatively clean, with activity associated almost exclusively with this mode, with only small contributions from $^+21^1$ when exciting via 19^1m^0, and $^+30^2$ when exciting via 19^1m^1. (The $^+30^1m^2$ contribution, seen when exciting via 19^1m^1 is consistent with the observation of this band when exciting via m^1 – see Refs. 7 and 14.) We observe that the wavenumber of $^+21^1m^0$ is very close to that of $^+m^5$; however, the latter is symmetry forbidden when exciting via 19^1m^0. (Although we have discussed previously[6] the possible activity of $^+m^5$ when exciting via m^0 for *m*FT in terms of a possible deviation away from the G_6 MSG, we currently favour the $^+21^1m^0$ assignment here.) On the other hand, it is clear that there is significant cross activity between 18^1 and 20^1, although this is much clearer when exciting via the $m = 0$ components: for the $m = 1$ components, the spectra are less clean and there are severely overlapped features (see Figure 5). In particular, 20^1m^0 is overlapped by 19^1m^1 for the ^{35}Cl isotopologue, as is evident from the REMPI spectra of the ^{35}Cl and ^{37}Cl isotopologues, Figure 1 (bottom trace). It can also be seen from Figure 1 that 20^1m^1 for

the ^{35}Cl isotopologue is overlapped by 20^1m^0 for the ^{37}Cl isotopologue, but we cannot see definitive evidence for the latter in the ZEKE spectra. No attempts were made to record ZEKE spectra via 20^1m^1 for the ^{37}Cl isotopologue.

We comment that the activity seen in the ZEKE spectra when exciting via 19^1m^0 and 19^1m^1 is similar to that observed[7] via the pure torsional levels, m^0 and m^1, although the $^+19^1m^x$ bands are relatively more intense here, as expected. We highlight that no evidence was seen for the $^+18^1m^x$ bands observed via the pure torsional levels;[7] additionally, there was a similar lack of $^+20^1m^x$ band activity. This suggests that the D_{19} vibration in the cation has a very similar motion to that of the S_1 state, which is largely supported by the Duschinsky matrix shown in Figure 6. In contrast, when exciting via 18^1m^0 and 18^1m^1 then bands attributable to both $^+18^1m^x$ and $^+20^1m^x$ are present, which is in line with the Duschinsky matrix. That said, the activity of $^+18^1m^x$ bands when exciting via 20^1m^1 is less clear, although there is plausible evidence for presence of a $^+18^1m^{3(+)}$ band when exciting via 20^1m^0. Since some of the $^+19^1m^x$ and $^+20^1m^x$ bands are very close in wavenumber, it is possible that $^+19^1m^x$ bands are hidden, but these are not expected, according to the Duschinsky matrix. Concomitantly, when exciting via 20^1m^0 and 20^1m^1, both $^+18^1m^x$ and $^+20^1m^x$ activity is present. The implication is that the D_{18} and D_{20} vibrations undergo Duschinsky mixing between the S_1 state and the cation, in line with the presented S_1/D_0^+ Duschinsky matrix.

From Figure 1, the 20^1m^0 transition is expected to be largely coincident with the 19^1m^1 transition for the ^{35}Cl isotopologue. The strongest ZEKE band expected from 20^1m^0 is $^+20^1m^{3(+)}$; this can be seen as a shoulder on the lower wavenumber side of the $^+19^1m^4$ band in Figure 5, providing evidence for this overlap. Similarly, the 19^1m^0 band for the ^{37}Cl isotopologue is mostly overlapping the same band for the ^{35}Cl isotopologue; but since we do not expect significant isotopic shifts for the $^+19^1m^x$ bands, then there is not expected to be any obvious evidence expected for this overlap, and indeed none is seen. We also note that the 20^1m^0 band for the ^{37}Cl isotopologue is expected to coincide with the 20^1m^1 band for the ^{35}Cl isotopologue, and there is a slight broadening of the main $^+20^1m^4$ band, but this is merely consistent with $^+20^1m^{3(+)}$ activity from the ^{37}Cl isotopologue, rather than being definitive.

Comparing the vibrational motions of the three vibrations shown in Figure 4 and Figure 6, it is clear that in the S_0 and D_0^+ states, the C-CH_3 and C-Cl stretches have become more localized for *m*ClT – as per the discussion given in Ref. 15 – see the forms of the D_{18} and D_{19} modes; however, there is more bending motion of the methyl group in D_{19} of *m*ClT caused by the more pronounced asymmetry in mass in the molecule.

In summary, between the S_1 and D_0^+ states for *m*ClT, the corresponding Duschinsky matrix suggests that all three of the D_{18}, D_{19} and D_{20} states undergo a small amount of Duschinsky mixing so that activity in each of the three modes is expected in the cation, whichever is excited, and this will, of course, apply to both of the $m = 0$ and $m = 1$ components. The spectra recorded when exciting via $18^1m^{0,1}$ do support a greater mixing between D_{18} and D_{20}. The spectra recorded when exciting via $19^1m^{0,1}$ appear to show little evidence of activity involving the other two vibrations, while those recorded via $20^1m^{0,1}$ suffer from significant overlap, but do not exclude involvement of activity of the other two vibrations. Hence, these observations are only qualitatively in line with the Duschinsky matrices. Overall, however, the situation for *m*ClT appears to be clearer cut than for *m*FT. We note our discussion of the geometry changes for *m*FT in Section III.C, which complicates the expected vibrational activity, and which also applies, but to a more limited extent, to *m*ClT. We highlight the consistency between the molecules with the activity of 18^1, 19^1 and 20^1 in the $S_1 \leftarrow S_0$ excitation (Figure 1). Further, we saw activity of both $^+18^1$ and $^+19^1$ when exciting via the vibrationless m^0 and m^1 levels,[7] which is expected from the anticipated changes in bond lengths; note that only $^+18^1$ was active in the case of *m*FT,[6] again illustrating activity differences between two very similar molecules.

IV. FURTHER DISCUSSION

A. Duschinsky rotation

The assumed linear and orthogonal relationship between the vibrations of different electronic states,[5] is only an approximation[26] and neither of these conditions strictly holds; moreover, when the geometries of the electronic states differ from each other, axis switching can occur,[27] which can further complicate the matter. On top of this, the entries in a Duschinsky matrix are a single number summarizing all of the changes in angular and radial motions of the bonds between two electronic states. If the vibrational motions are largely similar, then the diagonal entries will be the largest. If some of the vibrations become very mixed, then significant off-diagonal elements will be present, but still the diagonal elements would be expected to be the largest. The case is unusual here in that some off-diagonal elements are the largest for particular vibrations. Normally, this would suggest a misassignment of the vibrational labels; however, here these labels have been established from the S_0/D_0^+ Duschinsky matrix. Hence we interpret these large off-diagonal elements as reflecting particular aspects of the geometry changes that occur as a result of the electronic excitation. In such a scenario, as happens here for *m*FT, there is no longer a clear 1:1 correspondence between the vibrations in the S_1 state and the other two states. This is indeed largely borne out by the calculated matrices and the experimental observations as discussed in the present work, with the strong mixing between the D_{19}

and D_{20} modes for *m*FT being the most notable, and that between D_{18} and D_{20} being significant for *m*ClT.

Different Duschinsky mixings between the molecules will arise from the slightly different motions of the vibrations, owing to the different masses of the halogen atoms in the two cases, plus slightly different electronic effects caused by the different electronegativities of the halogen atoms, and the different overlap of the halogen orbitals with the aromatic π system. For *m*FT, the motions of two of the S_1 vibrations become strong mixtures of the S_0 (and D_0^+) vibrations, preventing the same labels being used; although the mixing is also significant for *m*ClT, the motions are similar enough to employ the same labels. These changes in motions are reflected in the activity in the ZEKE spectra and, for *m*FT, also in the 2D-LIF spectra.

B. Vibtor coupling and torsional potential changes

In Table III and Table IV, we give the wavenumbers of the different vibtor transitions in the cation for *m*FT and *m*ClT, respectively, and the separation of each of these levels from the m = 0 level of each vibration. Previously,[6,7] we have discussed the fact that the torsional potential of the out-of-plane D_{30} vibration and its first overtone in the cation is altered compared to the pure torsional potential for both *m*FT and *m*ClT, while the potentials for the observed in-plane (totally-symmetric) vibrations were not affected. Here, we find that the vibtor spacings of the cation involving the in-plane D_{19} vibration are reduced compared to those of the pure torsional levels (Table IV) suggesting the torsional barrier experienced during this vibration is lower, while some of those involving D_{20} are largely unaltered. However, it is difficult to rationalize, from the vibrational motions shown in Figure 4 and Figure 6, why the CH_3 torsional barrier is particularly sensitive to the D_{19} vibrational motion in the cation, and this may reflect a more complicated explanation in terms of electronic- and vibration-induced steric interactions.

V. CONCLUSIONS

In this work, we have focused on the activity and character of three vibrations for the closely-related molecules, *m*FT and *m*ClT. In particular, we examined the change in the character of a subset of the vibrations upon electronic excitation, $S_1 \leftarrow S_0$, which was deduced via the activity in ZEKE spectra, but also in 2D-LIF spectra for *m*FT. Even though the activity in the REMPI spectra was very similar for these two molecules, the details of the changing vibrational character showed that in fact there were significant differences in the mixings occurring as a result of electronic excitation and ionization. This could be seen from the calculated form of the vibrations, as well as the differences in the vibrational activity exhibited in the spectra. In general terms, the calculated Duschinsky matrices were in line with

the observed spectral activity, even though such matrices are only expected to be approximate reflections of the vibrational character change between electronic states. Unusually, for *m*FT, if one were to deduce the correspondence between the S_1 vibrations and those in the S_0 and D_0^+ states, reverse conclusions would be reached. This was identified as being due to the motions of the carbon atoms in the aromatic ring pairing with the switched C-CH_3 and C-F bond motions in the S_1 state for two of the vibrations. Remarkably, the Duschinsky matrices picked up the subtlety of the different electronic transitions affecting different geometric aspects of the molecule, and, in a qualitative way, correctly predicted the switched intensities of the transitions involving the D_{19} and D_{20} vibrations. We conclude that Duschinsky matrices, even though they are a rather coarse distillation of all of the changes in atomic motions between electronic states, are actually very sensitive to the aspects of the geometry that are most affected by the electronic transition.

Understanding such changes in detail, via assignment of vibrational structure as a result of electronic excitation and photoionization, are clearly key to understanding photo-physico-chemical behaviour.

Acknowledgements

We are grateful to the EPSRC for funding (grant EP/L021366/1). L.G.W. is grateful for an Undergraduate Summer Bursary funded via a University of Nottingham School of Chemistry 1960 scholarship. The EPSRC and the University of Nottingham are thanked for studentships to D.J.K. and A.R.D.

Data Availability Statement

The data that support the findings of this study are available from the corresponding author upon reasonable request.

Table I: Correspondence of the C_s point group symmetry classes with those of the G_6 molecular symmetry group. Also indicated are the symmetries of the D_i vibrations and the different pure torsional levels.[a]

C_s	G_6	D_i[b]	m
a'	a_1	D_1–D_{21}	0, 3(+),6(+), 9(+)
a''	a_2	D_{22}–D_{30}	3(-),6(-), 9(-)
	e		1,2,4,5,7,8

[a] Symmetries of vibtor levels can be obtained by combining the vibrational symmetry (in G_6) with those of the pure torsional level, using the C_{3v} point group direct product table.

[b] The D_i labels are described in Ref. 15, where the vibration mode diagrams can also be found.

Table II: Calculated and experimental wavenumbers for *m*FT and *m*ClT vibrations pertinent to the present study.

D_i	S_0		S_1		D_0^+	
	Calculated[a]	Experimental	Calculated[b]	Experimental	Calculated[c]	Experimental
*m*FT						
17	718	728[d, f]	685	685[d,f]	700	
18	519	527[d,f,g]	459	460 [e,f]	509	510[e,f]
19 (X)	505	512[d,f,g]	448	457[d,e,f]	410	415[f]
20 (Y)	435	445 [d,f,g]	410	420[d,e,f]	442	456[f]
21	285	292 [d,f,g]	281	284[d,e,f,g]	290	296 [e,f]
28	443	438 [d,f,g]	241	258[d,e,f,g]	373	375 [e,f]
29	236	236[f,g]	184	173 [d,e,f,g]	190	190 [e,f]
30	199	201[f,g]	122	127 [d,e,f,g]	167	167 [e,f]
*m*ClT						
18	513	524 [h,j]	446	455[h]	455	457[i]
19	402	409 [h,j]	373	378[h]	391	396[i]
20	376	387 [h,j]	368	373[h]	377	387[i]
21	226	221 [h,j]	226	231[i]	233	240[i]
28	432	431[j]	241		366	
29	213	234[j]	159	151[i]	176	176[i]
30	171	185[j]	80	111[i]	150	149[i]

[a] B3LYP/aug-cc-pVTZ, scaled by 0.97. For *m*ClT, the results are for the ^{35}Cl isotopologue.

[b] TD-B3LYP/aug-cc-pVTZ, scaled by 0.97. For *m*ClT, the results are for the ^{35}Cl isotopologue.

[c] UB3LYP/aug-cc-pVTZ, scaled by 0.97; $\langle S^2 \rangle = 0.76$. For *m*ClT, the results are for the ^{35}Cl isotopologue.

[d] Ref. 9. Small updates to some of these values have been made in Refs. 3, 8 and the present work.

[e] Ref. 6

[f] Present work. The experimental values for D_{27} were obtained from observed vibtor bands. In the case of D_{19} and D_{20} in the S_1 state, which we have designated D_X and D_Y in the text, we have allocated these to the D_i label that has the maximum S_0 contribution from the Duschinsky matrix in Figure 4.

[g] From Ref. 8

[h] From Ref. 13

[i] From Ref. 7

[j] Ref. 15.

Table III: Separations of vibtor levels built on different vibrations for *m*FT (cm^{-1}).

	Vibrational Level[a,b]			
Torsion[c]	$^{+}0^{0}$ [0]	$^{+}18^{1}$ [510]	$^{+}19^{1}$ [415]	$^{+}20^{1}$ [456]
$^{+}m^{0,1}$	0	0	0	0
$^{+}m^{2}$	101	100 (610)	94 (509)	102 (558)
$^{+}m^{3(-)}$	103	102 (612)		
$^{+}m^{3(+)}$	185	184 (694)	172 (587)	187 (643)
$^{+}m^{4}$	192	193 (703)	181 (596)	195 (651)
$^{+}m^{5}$	250	250 (760)	235 (650)	254 (710)
$^{+}m^{6(-)}$	292	292 (802)		294 (750)
$^{+}m^{6(+)}$	311	312 (822)	293 (708)	312 (768)
$^{+}m^{7}$	368	370 (880)		

[a] Torsional spacings are given with respect to the band position of the $m = 0$ level of the indicated vibration.

[b] Values in square brackets in the column headers are the wavenumbers of the $m = 0$ level of the indicated vibration.

[c] The $^{+}m^{0}$ and $^{+}m^{1}$ levels are degenerate at our resolution. Levels with $m \neq 3n$ have degenerate + and – levels.

Table IV: Separations of vibtor levels built on different vibrations for *m*ClT (cm^{-1}).

	Vibrational Level[a,b]			
Torsion[c]	$^{+}0^{0}$ [0]	$^{+}18^{1}$ [457]	$^{+}19^{1}$ [396]	$^{+}20^{1}$ [387]
$^{+}m^{0,1}$	0	0	0	0
$^{+}m^{2}$	98	97 (555)	94 (490)	105 (492)
$^{+}m^{3(-)}$	98			
$^{+}m^{3(+)}$	175	177 (633)	171 (563)	182 (569)
$^{+}m^{4}$	186	186 (642)	177 (573)	193 (584)
$^{+}m^{5}$	246	248 (704)	240 (636)	254 (641)
$^{+}m^{6(-)}$	284	278 (734)	272 (668)	
$^{+}m^{6(+)}$	300	300 (756)	294 (690)	300 (687)
$^{+}m^{7}$	363			

[a] Torsional spacings are given with respect to the band position of the $m = 0$ level of the indicated vibration. The values in parentheses are the actual band position with respect to $^{+}m^{0}$.

[b] Values in square brackets in the column headers are the wavenumbers of the $m = 0$ level of the indicated vibration.

[c] The $^{+}m^{0}$ and $^{+}m^{1}$ levels are degenerate at our resolution. Levels with $m \neq 3n$ have degenerate + and – levels.

Figure Captions

Figure 1: REMPI spectra of the 0–500 cm^{-1} region above the origin for the $S_1 \leftarrow S_0$ transition for (a) *m*FT and (b) *m*ClT. In each case, the expanded views of the regions corresponding to the $18^1m^{0,1}$, $19^1m^{0,1}$ and $20^1m^{0,1}$ transitions are shown. In the case of *m*ClT, traces for both the ^{35}Cl and ^{37}Cl isotopologues are presented. Note that for *m*FT, the region around the origin to lower wavenumber than the indicated break has been scaled by a factor of 0.5.

Figure 2: 2D-LIF spectrum for *m*FT, where the excitation range covers the $18^1m^{0,1}$, $19^1m^{0,1}$ and $20^1m^{0,1}$ transitions. The emission range covers the main $\Delta(v, m) = 0$ regions, extending to higher wavenumber to include other key features. Assignments for related bands (e.g. vibtor and combination levels of the same vibration) are shown in the same colour. Features marked with an asterisk are not assigned here, but these will be addressed in a future publication.

Figure 3: ZEKE spectra of *m*FT recorded at different $S_1 \leftarrow S_0$ excitation positions, separated into $m = 0$ and $m = 1$ components. For clarity, the preceding superscripted "+" used in the text is omitted from the transition labels. Since the 18^1m^1 and 19^1m^0 transitions are overlapping, the corresponding ZEKE spectrum has been included in both parts of the figure; the bold label indicates the pertinent level for that part of the figure. We have added obeli (†) to bands that arise from the overlapping transition, and which are labelled on the duplicate trace. The relative energy scales are given with respect to the $^+m^0$ and $^+m^1$ transitions; in absolute terms, the $^+m^1$ transition is ca. 5 cm^{-1} lower in wavenumber, owing to the $m_1 \leftarrow m_0$ spacing in the S_0 state.

Figure 4: Top. Duschinsky matrices for selected vibrations of *m*FT for combinations of the S_0, S_1 and D_0^+ electronic states. The depth of grey shading represents the coefficients of the mixing between the vibrations in the two electronic states, with white representing 0 and black representing 1. Bottom. Calculated mode diagrams for the three vibrations corresponding to D_{18}, D_{19}, and D_{20} in the three different electronic states. See text for further discussion.

Figure 5: ZEKE spectra of *m*ClT recorded at different $S_1 \leftarrow S_0$ excitation positions, separated into $m = 0$ and $m = 1$ components. For clarity, the preceding superscripted "+" used in the text is omitted from the transition labels. Since the 19^1m^1 and 20^1m^0 transitions are overlapping, the corresponding ZEKE spectrum has been included in both parts of the figure; the bold label indicates the pertinent level for that part of the figure. We have added obeli (†) to bands that arise from the overlapping transition, and which are labelled on the duplicate trace. The low-wavenumber bands marked with asterisks (*) are spurious. The relative energy scales are given with respect to the $^+m^0$ and $^+m^1$ transitions; in

absolute terms, the $^{+}m^{1}$ transition is ca. 5 cm^{-1} lower in wavenumber, owing to the $m_1 \leftarrow m_0$ spacing in the S_0 state.

Figure 6: Top. Duschinsky matrices for *m*ClT between combinations of the S_0, S_1 and D_0^+ electronic states. The depth of grey shading represents the coefficients of the mixing between the vibrations in the two electronic states, with white representing 0 and black representing 1. Bottom. Calculated mode diagrams for the three vibrations corresponding to D_{18}, D_{19}, and D_{20} in the three different electronic states. See text for further discussion.

Figure 1

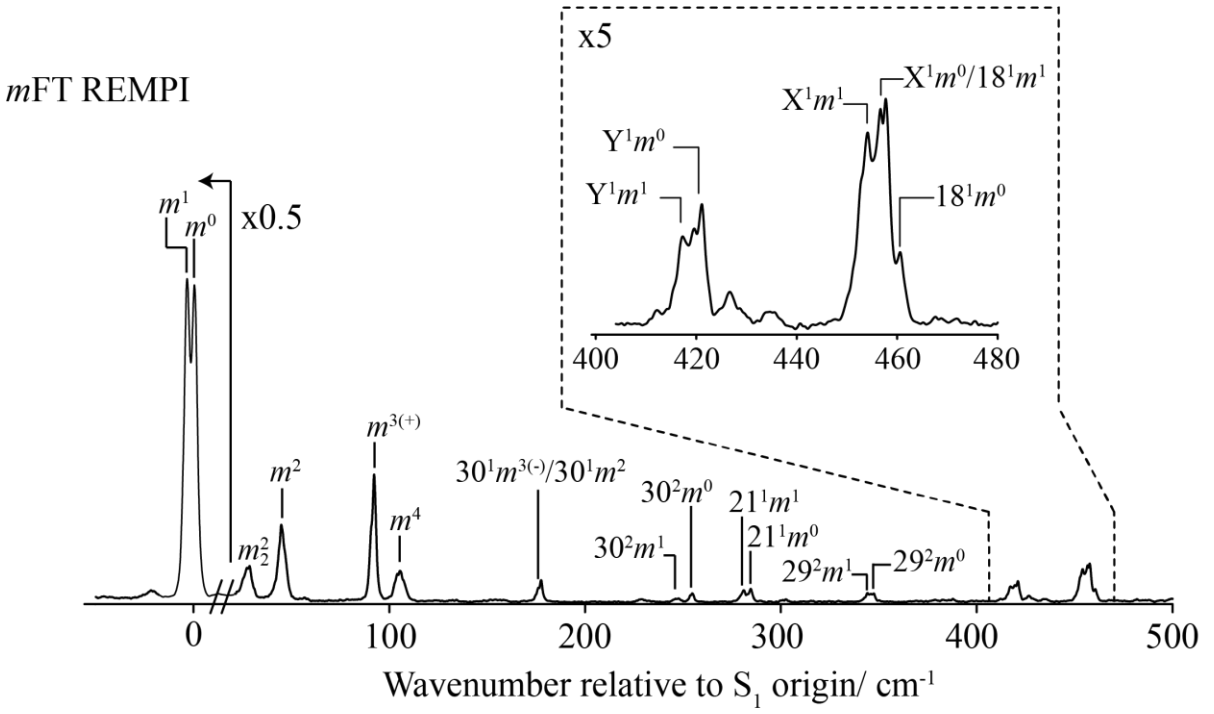
mFT REMPI
x5
X¹m¹
X¹m⁰/18¹m¹
Y¹m⁰
Y¹m¹
18¹m⁰
400
420
440
460
480
m¹
m⁰
x0.5
m²
m³(+)
m⁴
m₂²
30¹m³(-)/30¹m²
30²m⁰
21¹m¹
21¹m⁰
30²m¹
29²m¹
29²m⁰
0
100
200
300
400
500
Wavenumber relative to S1 origin/ cm-1

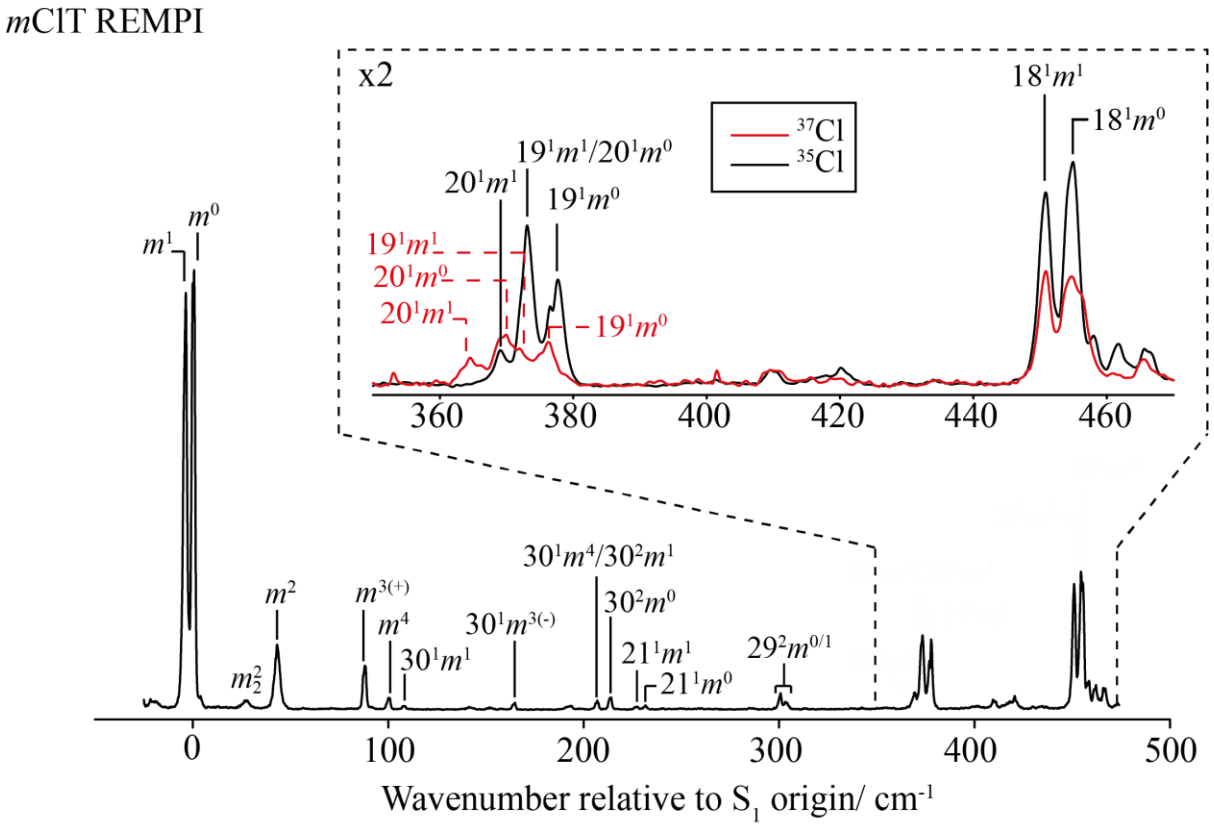
mClT REMPI
x2
37Cl
35Cl
18¹m¹
18¹m⁰
19¹m¹/20¹m⁰
20¹m¹
19¹m⁰
19¹m¹
20¹m⁰
20¹m¹
19¹m⁰
360
380
400
420
440
460
m¹
m⁰
m²
m³(+)
m⁴
m₂²
30¹m⁴/30²m¹
30²m⁰
30¹m³(-)
30¹m¹
21¹m¹
21¹m⁰
29²m⁰/¹
0
100
200
300
400
500
Wavenumber relative to S1 origin/ cm-1

Figure 2

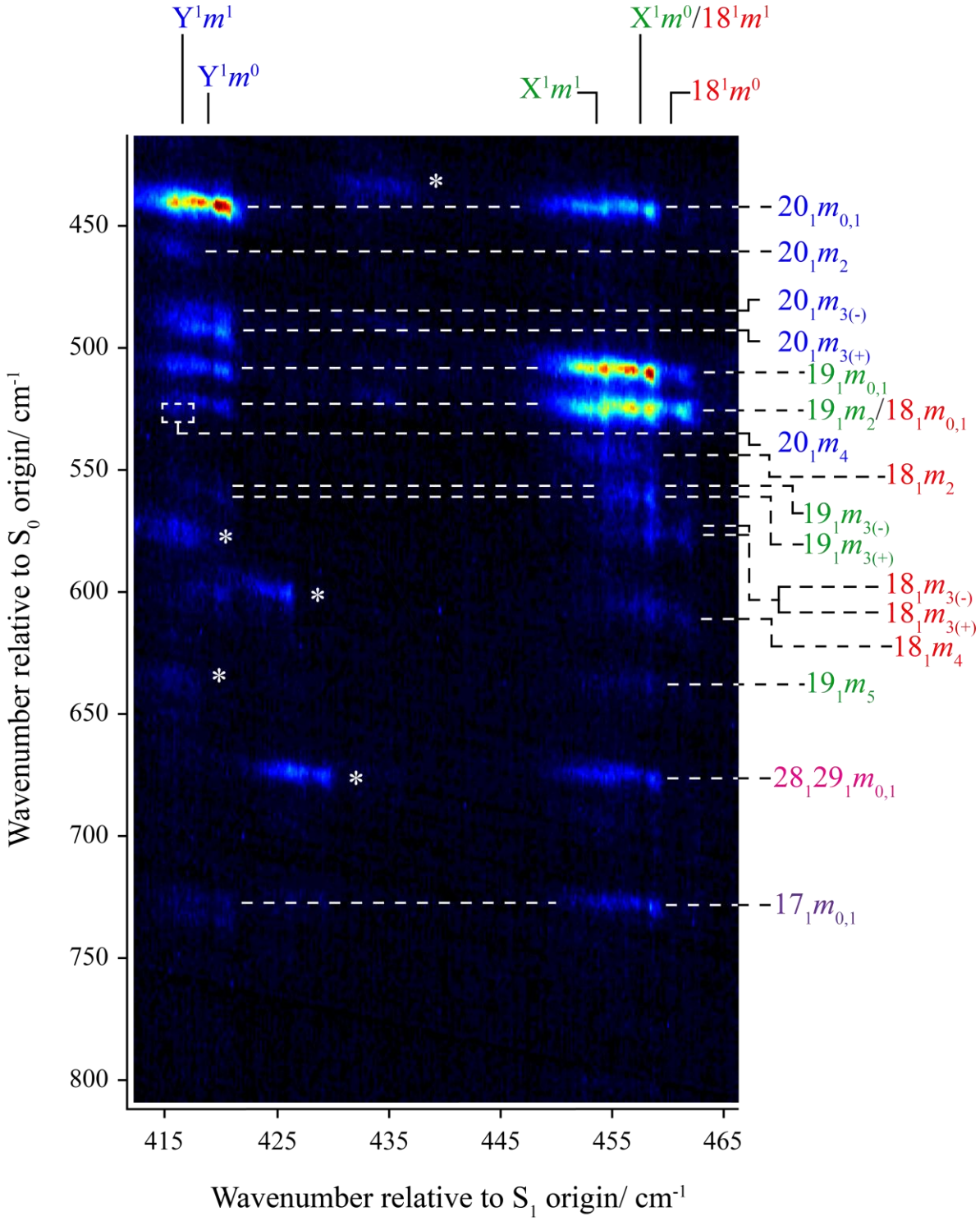
Y1m1
Y1m0
X1m1
X1m0/181m1
181m0
20 1m0,1
20 1m2
20 1m3(-)
20 1m3(+)
19 1m0,1
19 1m2/18 1m0,1
20 1m4
18 1m2
19 1m3(-)
19 1m3(+)
18 1m3(-)
18 1m3(+)
18 1m4
19 1m5
28 129 1m0,1
17 1m0,1
Wavenumber relative to S0 origin/ cm-1
Wavenumber relative to S1 origin/ cm-1
450
500
550
600
650
700
750
800
415
425
435
445
455
465

Figure 3

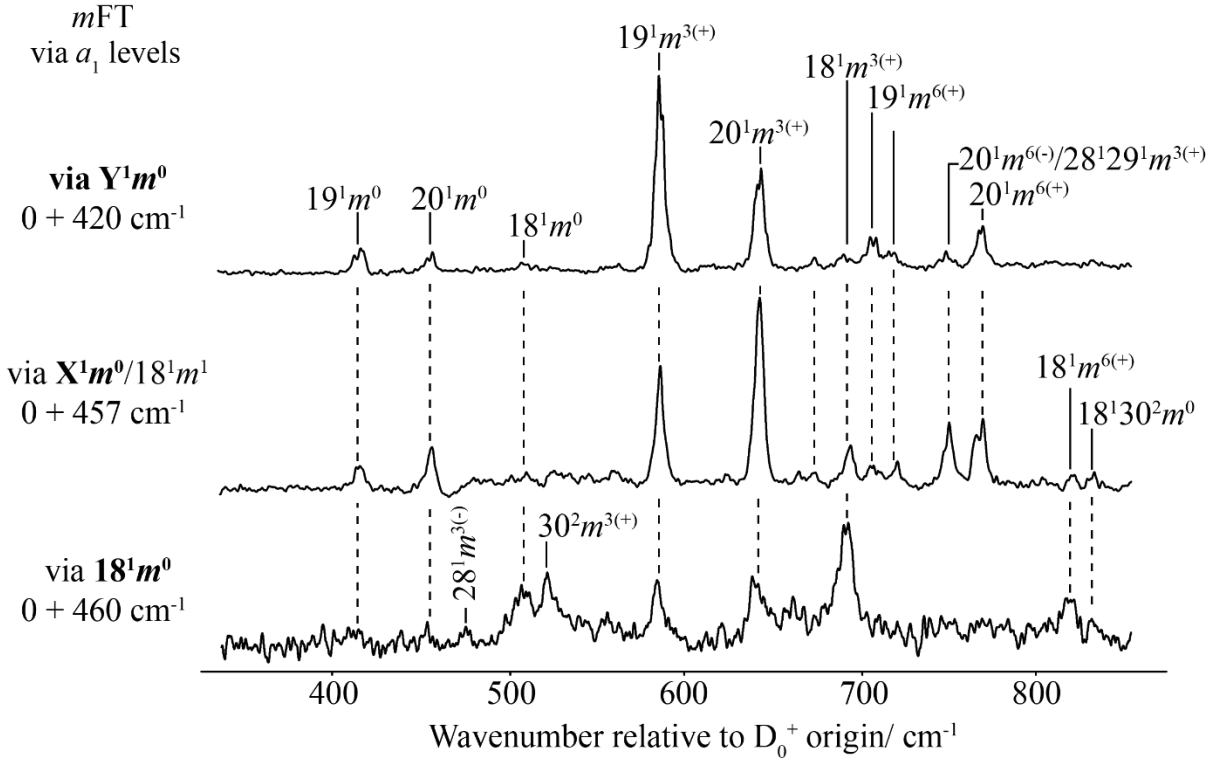
mFT
via a_1 levels
via $\mathbf{Y^1}\boldsymbol{m^0}$
0 + 420 cm^{-1}
via $\mathbf{X^1}\boldsymbol{m^0}$/$18^1m^1$
0 + 457 cm^{-1}
via $\mathbf{18^1}\boldsymbol{m^0}$
0 + 460 cm^{-1}
19^1m^0
20^1m^0
18^1m^0
$19^1m^{3(+)}$
$20^1m^{3(+)}$
$18^1m^{3(+)}$
$19^1m^{6(+)}$
$20^1m^{6(-)}/28^129^1m^{3(+)}$
$20^1m^{6(+)}$
$18^1m^{6(+)}$
$18^130^2m^0$
$28^1m^{3(-)}$
$30^2m^{3(+)}$
400
500
600
700
800
Wavenumber relative to D_0^+ origin/ cm^{-1}

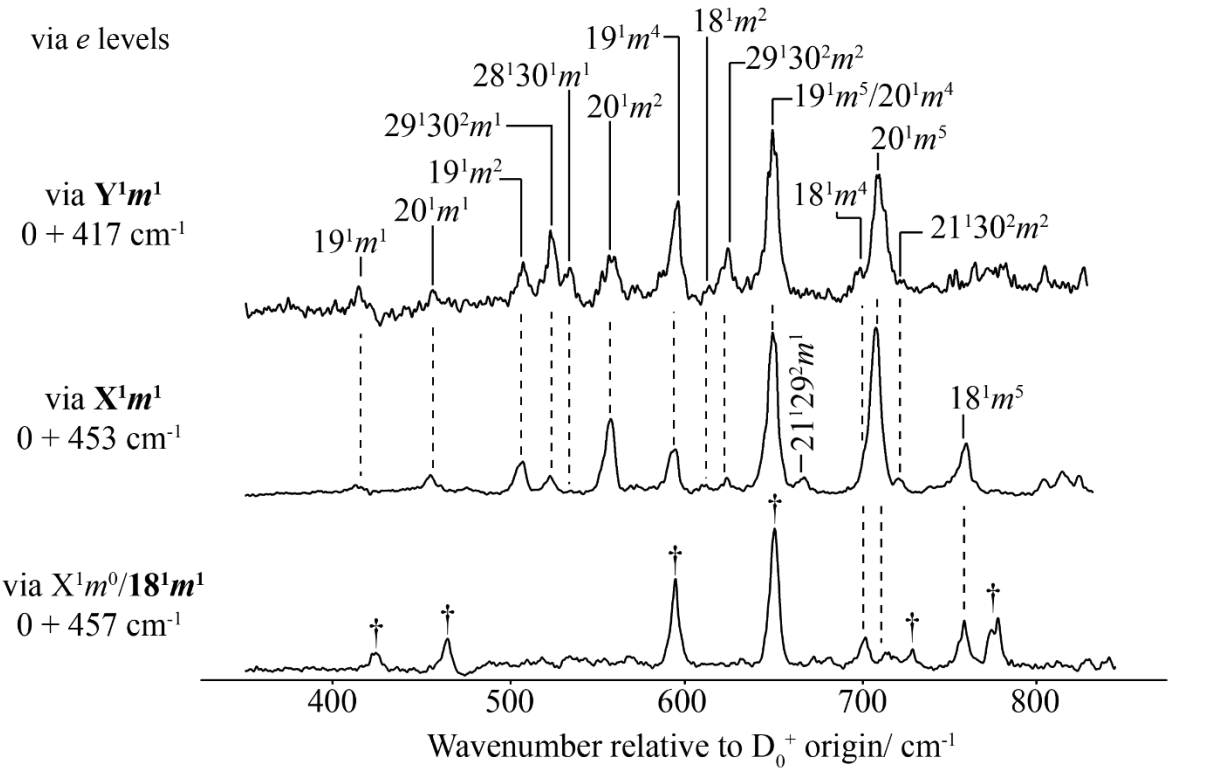
via e levels
via $\mathbf{Y^1}\boldsymbol{m^1}$
0 + 417 cm^{-1}
via $\mathbf{X^1}\boldsymbol{m^1}$
0 + 453 cm^{-1}
via $X^1m^0/\mathbf{18^1}\boldsymbol{m^1}$
0 + 457 cm^{-1}
19^1m^1
20^1m^1
19^1m^2
$29^130^2m^1$
$28^130^1m^1$
20^1m^2
19^1m^4
18^1m^2
$29^130^2m^2$
$19^1m^5/20^1m^4$
20^1m^5
18^1m^4
$21^130^2m^2$
$21^129^2m^1$
18^1m^5
†
400
500
600
700
800
Wavenumber relative to D_0^+ origin/ cm^{-1}

Figure 4

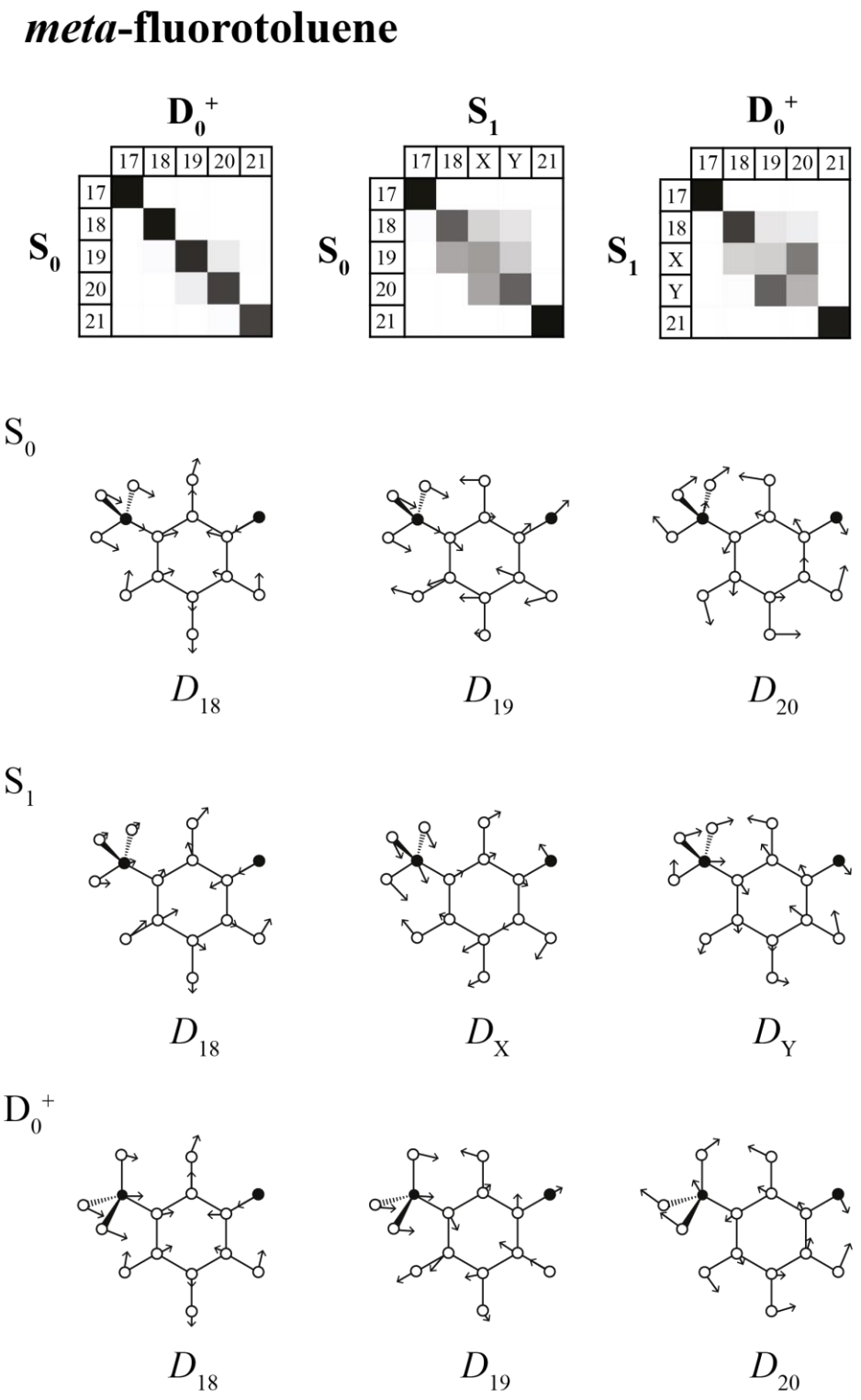
meta-fluorotoluene
D0+
S1
D0+
17 18 19 20 21
17 18 X Y 21
17 18 19 20 21
S0
S0
S1
17
18
19
20
21
X
Y
S0
D18
D19
D20
S1
D18
DX
DY
D0+
D18
D19
D20

Figure 5

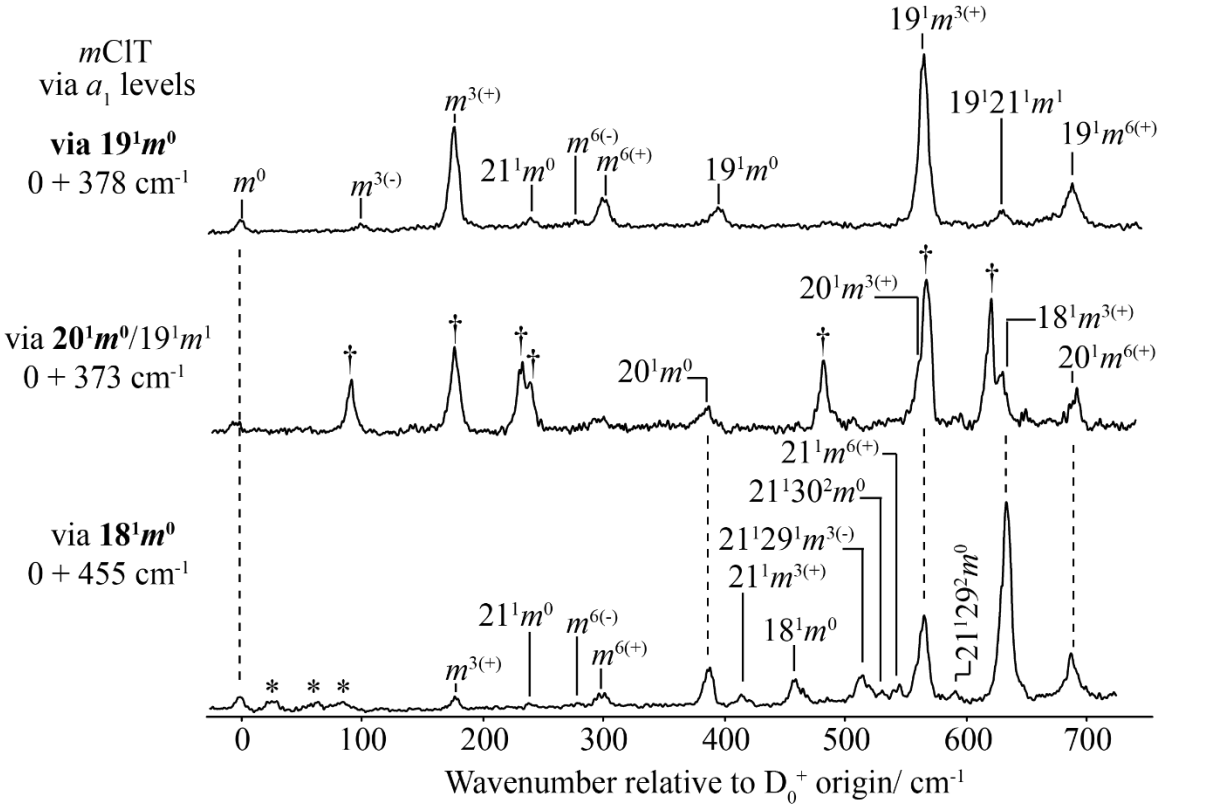
mClT
via a_1 levels
via 19^1m^0
0 + 378 cm^{-1}
via 20^1m^0/19^1m^1
0 + 373 cm^{-1}
via 18^1m^0
0 + 455 cm^{-1}
m^0
$m^{3(-)}$
$m^{3(+)}$
21^1m^0
$m^{6(-)}$
$m^{6(+)}$
19^1m^0
$19^1m^{3(+)}$
$19^121^1m^1$
$19^1m^{6(+)}$
$20^1m^{3(+)}$
$18^1m^{3(+)}$
$20^1m^{6(+)}$
20^1m^0
$21^1m^{6(+)}$
$21^130^2m^0$
$21^129^1m^{3(-)}$
$21^1m^{3(+)}$
18^1m^0
$21^129^2m^0$
0
100
200
300
400
500
600
700
Wavenumber relative to D_0^+ origin/ cm^{-1}

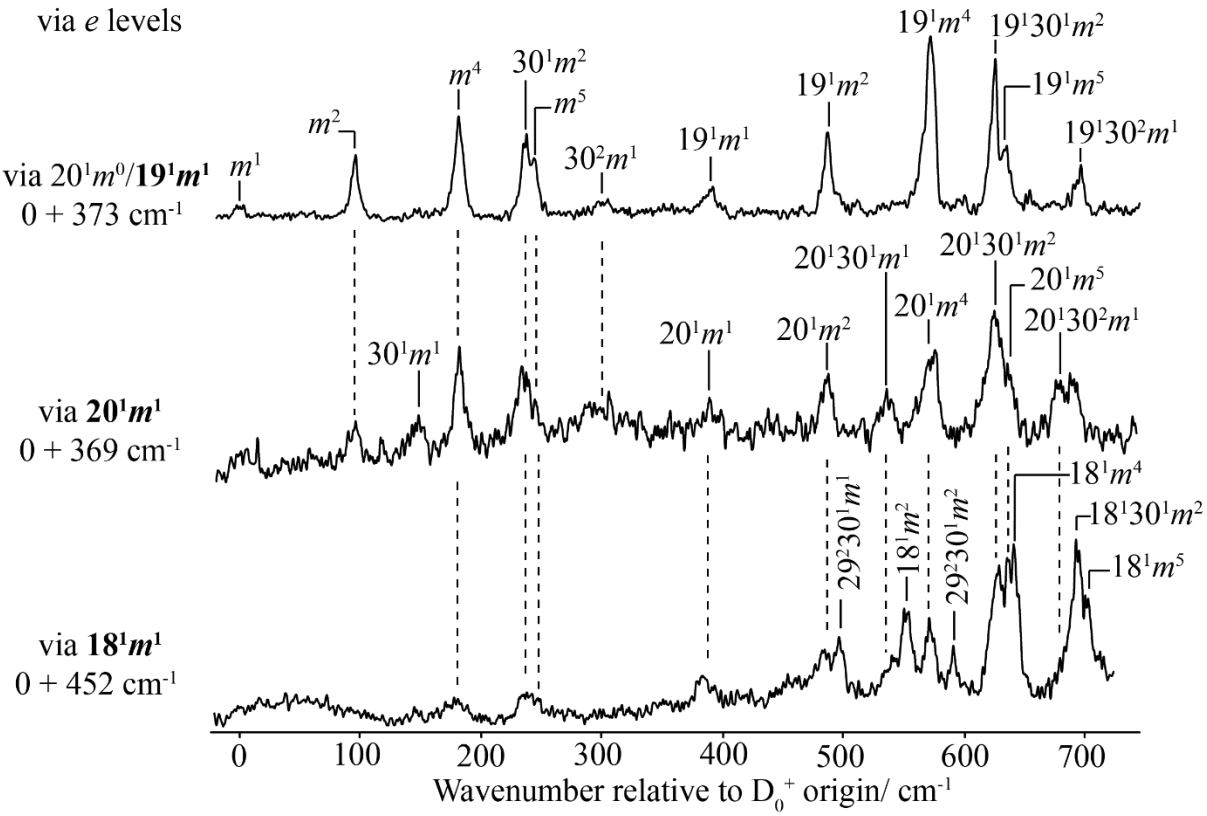
via e levels
via 20^1m^0/19^1m^1
0 + 373 cm^{-1}
via 20^1m^1
0 + 369 cm^{-1}
via 18^1m^1
0 + 452 cm^{-1}
m^1
m^2
m^4
30^1m^2
m^5
30^2m^1
19^1m^1
19^1m^2
19^1m^4
$19^130^1m^2$
19^1m^5
$19^130^2m^1$
30^1m^1
20^1m^1
20^1m^2
$20^130^1m^1$
20^1m^4
$20^130^1m^2$
20^1m^5
$20^130^2m^1$
18^1m^4
$18^130^1m^2$
18^1m^5
$29^230^1m^1$
18^1m^2
$29^230^1m^2$
0
100
200
300
400
500
600
700
Wavenumber relative to D_0^+ origin/ cm^{-1}

Figure 6

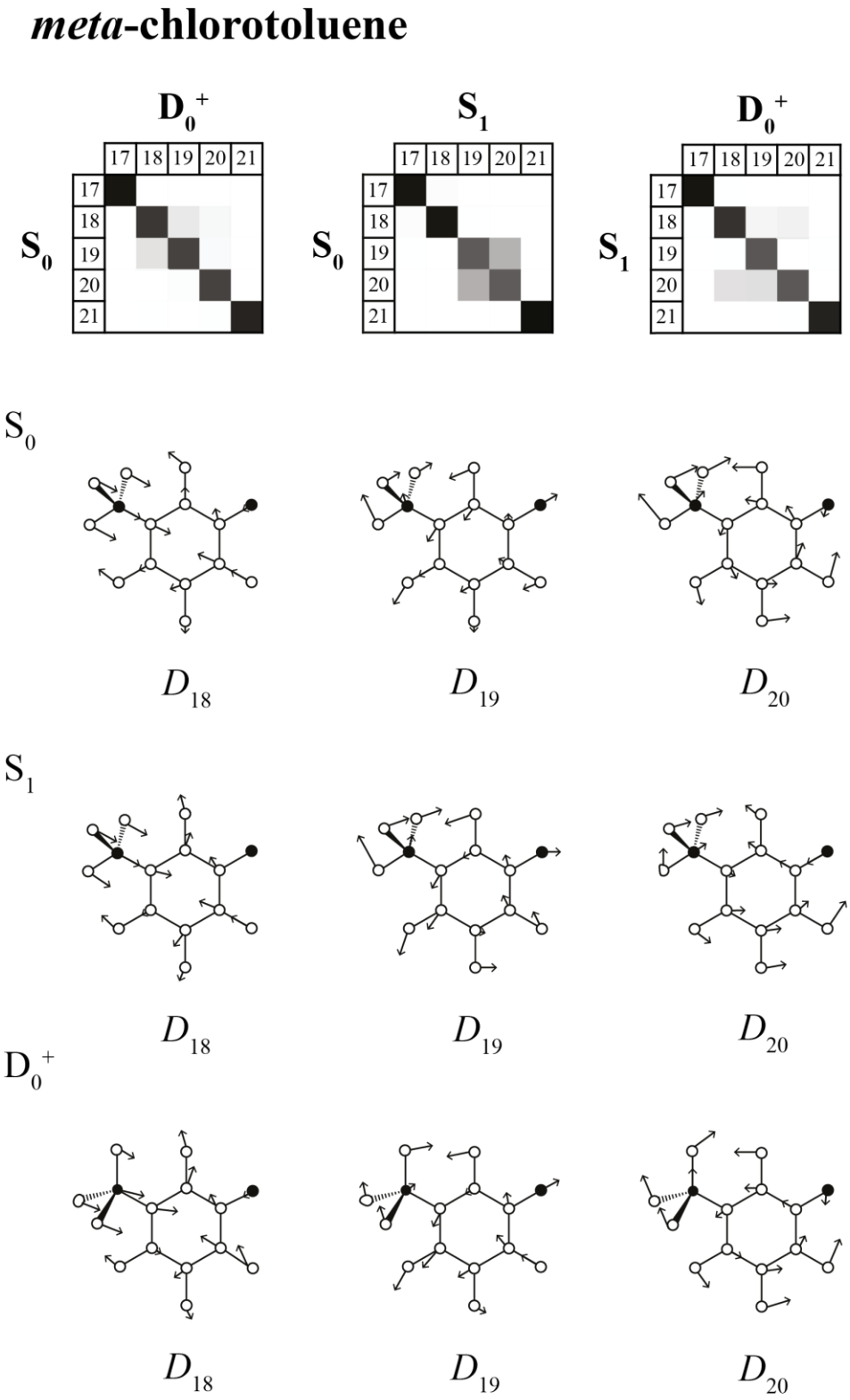
meta-chlorotoluene
D0+
S1
D0+
17 18 19 20 21
S0
S0
S1
S0
S1
D0+
D18
D19
D20
D18
D19
D20
D18
D19
D20

References

[1] D. J. Nesbitt and R. W. Field, J. Phys. Chem. **100**, 12735 (1996).

[2] G. M. Roberts and V. G. Stavros, in "Ultrafast Phenomena in Molecular Sciences", ed. R. de. Balda and L. Bañares, Springer, Dordrecht (2014).

[3] Y. He, C. Wu, and W. Kong, J. Phys. Chem. A **107**, 5145 (2003).

[4] C. Skinnerup Byskov, F. Jensen, T. J. D. Jørgensen, and S. B. Nielsen, Phys. Chem. Chem. Phys. **16**, 15831 (2014).

[5] F. Duschinsky, Acta Phys.-Chim. U.R.S.S. **7**, 551 (1937).

[6] D. J. Kemp, E. F. Fryer, A. R. Davies, and T. G. Wright, J. Chem. Phys. **151**, 084311 (2019).

[7] D. J. Kemp, L. G. Warner, and T. G. Wright, J. Chem. Phys. **152**, 064303 (2020).

[8] L. D. Stewart, J. R. Gascooke, and W. D. Lawrance, J. Chem. Phys. **150**, 174303 (2019).

[9] K. Okuyama, N. Mikami, and M. Ito, J. Phys. Chem. **89**, 5617 (1985).

[10] K. Takazawa, M. Fujii, T. Ebata, and M. Ito, Chem. Phys. Lett. **189**, 592 (1992).

[11] M. Ito, K. Takazawa, and M. Fujii, J. Molec. Struct. **292**, 9 (1993).

[12] K. Takazawa, M. Fujii, and M. Ito, J. Chem. Phys. **99**, 3205 (1993).

[13] T. Ichimura, A. Kawana, T. Suzuki, T. Ebata, and N. Mikami, J. Photochem. Photobiol. A: Chem. **80**, 145 (1994).

[14] S. H. Feldgus, M. J. Schroeder, R. A. Walker, W.-K. Woo, and J. C. Weisshaar, Int. J. Mass Spectrom. Ion. Proc. **159**, 231 (1996).

[15] D. J. Kemp, W. D. Tuttle, F. M. S. Jones. A. M. Gardner, A. Andrejeva, J. C. A. Wakefield, and T. G. Wright, J Mol. Spect. **346**, 46 (2018).

[16] V. L. Ayles, C. J. Hammond, D. E. Bergeron, O. J. Richards, and T. G. Wright, J. Chem. Phys. **126**, 244304 (2007).

[17] A. M. Gardner, W. D. Tuttle, L. E. Whalley, and T. G. Wright, Chem. Sci. **9**, 2270 (2018).

[18] N. J. Reilly, T. W. Schmidt, and S. H. Kable, J. Phys. Chem. A **110**, 12355 (2006).

[19] J. R. Gascooke and W. D. Lawrance, Eur. Phys. J. D **71**, 287 (2017).

[20] E. B. Wilson, Jr, Phys. Rev. **45**, 706, (1934).

[21] G. Varsányi, *Assignments of the Vibrational Spectra of Seven Hundred Benzene Derivatives*, Wiley, New York, 1974.

[22] R. S. Mulliken, J. Chem. Phys. **23**, 1997 (1955).

[23] G. Herzberg, *Molecular Spectra and Molecular Structure II. Infrared and Raman Spectra of Polyatomic Molecules*, Krieger, Malabar, 1991.

[24] A. M. Gardner, W. D. Tuttle, P. Groner, and T. G. Wright, J. Chem. Phys. **146**, 124308 (2017).

[25] I. Pugliesi and K. Muller-Dethlefs, J. Phys. Chem. A **110**, 4657 (2006). A free download of the software can be found at http://www.fclab2.net

[26] See, for example G. M. Sando and K. G. Spears, J. Phys. Chem. A **105**, 5326 (2001).

[27] J. T. Hougen and J. K. G. Watson, Can. J. Phys. **43**, 298 (1965).